An imaging-based diagnostic approach to vascular anomalies of the oral and maxillofacial region

WLLA E. AL-HAMMAD[1,2], MAMIKO FUJIKURA[3], MIKI HISATOMI[3], SHUNSUKE OKADA[3],
LUCIANA MUNHOZ[4], TOSHIYUKI KAWAZU[5], YOHEI TAKESHITA[5], MARIKO FUJITA[5],
YOSHINOBU YANAGI[6] and JUN-ICHI ASAUMI[3,5]

[1]Department of Oral and Maxillofacial Radiology, Graduate School of Medicine, Dentistry and Pharmaceutical Sciences,
Okayama University, Okayama 700-8558, Japan; [2]Department of Oral Medicine and Oral Surgery, Faculty of Dentistry,
Jordan University of Science and Technology, Irbid 22110, Jordan; [3]Department of Oral Diagnosis and Dentomaxillofacial
Radiology, Okayama University Hospital, Okayama 700-8558, Japan; [4]Department of Stomatology, School of Dentistry,
University of São Paulo, São Paulo 05508-000, Brazil; [5]Department of Oral and Maxillofacial Radiology,
Faculty of Medicine, Dentistry and Pharmaceutical Sciences, Okayama University, Okayama 700-8558;
[6]Department of Dental Informatics, Faculty of Medicine, Dentistry and Pharmaceutical Sciences,
Okayama University, Okayama 700-8525, Japan

Abstract. The accurate diagnosis of vascular anomalies (VAs) is considered a challenging endeavor. Misdiagnosis of VAs can lead clinicians in the wrong direction, such as the performance of an unnecessary biopsy or inappropriate surgical procedures, which can potentially lead to unforeseen consequences and increase the risk of patient injury. The purpose of the present study was to develop an approach for the diagnosis of VAs of the oral and maxillofacial region based on computed tomography (CT), magnetic resonance imaging (MRI) and dynamic contrast-enhanced MRI (DCE-MRI). In the present study, the CT and MR images of 87 VAs were examined, and the following imaging features were evaluated: Detectability of the lesion, the periphery of the lesion, the inner nature of the lesion, the density of the lesion on CT, the signal intensity of the lesion on MRI, the detectability of phleboliths and the shape of the lesion. A total of 29 lesions were further evaluated using the contrast index (CI) curves created from the DCE-MRI images. A diagnostic diagram, which is based on the imaging features of VAs and CI curve patterns, was subsequently extrapolated. The results obtained demonstrated that the VAs were detected more readily by MRI compared with CT, whereas the detectability of phleboliths was superior when using CT compared with MRI. VAs showed a propensity for homogeneous isodensity on CT, whereas, by contrast, they exhibited a propensity for heterogeneous hyperdensity on CE-CT. VAs also showed a propensity for homogeneous intermediate signal intensity when performing T1-weighted imaging (T1WI), heterogeneous high signal intensity when performing short tau inversion recovery MRI, and heterogeneous high signal intensity when performing fat-saturated CE-T1WI. The CI curves of VAs were found to exhibit a specific pattern: Of the 29 CI curves, 23 (79.3%) showed early weak enhancement, followed by a plateau leading up to 400-600 sec. An imaging-based diagnostic diagram was ultimately formulated. This diagram can act as an aid for radiologists when they are expecting to find a VA, and hopefully serve the purpose of simplifying the diagnostic process. Taken together, the findings of the present study indicated that DCE-MRI may be considered a useful tool for the diagnosis of VAs.

Introduction

Vascular anomalies (VAs) account for ~4.5% of head-and-neck lesions, and are usually diagnosed during infancy or childhood (1). The International Society for the Study of Vascular Anomalies has provided the most-used classification for VAs, dividing them into two major categories: Vascular tumors (defined as true proliferative neoplasms of endothelial cells) and vascular malformations (defined as defects of vascular morphogenesis/structural abnormalities) (2). Although examining the patient's history and proper clinical examination are frequently sufficient to diagnose VAs, there remain many cases in which a diagnosis cannot be made without radiological imaging. Magnetic resonance imaging (MRI) serves a vital role in diagnosing deep VAs, both demonstrating their extension and determining their anatomic association with adjacent structures for appropriate treatment guidance (3). Computed

Correspondence to: Dr Mamiko Fujikura, Department of Oral Diagnosis and Dentomaxillofacial Radiology, Okayama University Hospital, 2-5-1 Shikata-cho, Kita-ku, Okayama 700-8558, Japan
E-mail: fujikura@okayama-u.ac.jp

tomography (CT) is also helpful in the diagnosis of VAs due to its fast acquisition speed and wide availability, especially when urgent imaging is required; however, the exposure to ionizing radiation limits its usability, especially in pediatric patients (4,5). Previous studies have demonstrated MRI to be superior to CT as a technique with respect to the diagnosis and treatment planning of VAs due to its valuable contribution to tissue characterization and determination of lesion extension. However, the detectability of phleboliths is superior on CT compared with MRI (6-8).

The misdiagnosis of VAs can lead clinicians in the wrong direction, such as performing unnecessary biopsies or surgical procedures which in themselves may lead to unfavorable, life-threatening outcomes, such as massive bleeding. Therefore, the accurate and precise differentiation of VAs from other types of lesions is important for optimal patient care (9-11).

Recently, dynamic contrast-enhanced MRI (DCE-MRI) has been shown to have an important role in improving the diagnosis of several benign and malignant lesions of the oral and maxillofacial area through providing hemodynamic information on the lesion, including its regional blood volume, flow and vascular permeability (12-18). However, to the best of our knowledge, no previously published study has investigated the potential role of DCE-MRI contrast index (CI)-based parameters in the diagnosis of oral and maxillofacial VAs.

The present retrospective study therefore aimed to develop a more structured approach for the diagnosis of VAs based on CT and MRI features; furthermore, it sought to evaluate the diagnostic value of DCE-MRI for VAs of the oral and maxillofacial area.

Patients and methods

Patients. A total of 70 patients with 87 lesions were admitted to Okayama University Hospital between April 2012 and March 2023. These patients underwent CT and MRI imaging with a diagnosis of VA of the head-and-neck area. The diagnoses were based on both clinical examination and histopathological findings. The patients had a mean age of 43.2 years (age range: 2-82 years) and comprised 27 men and 43 women. MRI images were obtained for all 87 lesions, whereas DCE-MRI images were obtained for 45 lesions, among which nine lesions with a short scan time or motion artifacts were excluded. CT was acquired for 28 lesions, among which six lesions showing metal artifacts on imaging were excluded. Therefore, in this retrospective study, MRI was used to evaluate a total of 87 lesions, DCE-MRI was used to evaluate 36 lesions, and CT was used to evaluate 22 lesions.

CT protocol. CT images were acquired using one of four CT scanners: Aquilion™ ONE (Canon Medical Systems Corporation), SOMATOM Definition Flash (Siemens Healthineers), Aquilion™ Precision (Canon Medical Systems Corporation), or Discovery CT750 HD (GE Healthcare), with settings of 120 kV and 113-300 mA. On performing CT, lesions were evaluated using the axial plane with the X-ray beam parallel to the occlusal plane or the mandibular plane. The field of view was 24x24 cm, the matrix size was 512x512 pixels, and the slice thickness was 1-1.25 mm. For

contrast-enhanced (CE)-CT images, one of four types of non-ionic contrast material was used: Iopamidol (Iopamiron 300; Bayer Yakuhin, Ltd.), iohexol (Iopamiron 300; Daiichi Sankyo Co., Ltd.), iomeprol (Iomeron 300; Eisai, Co., Ltd.) or iopromide (Iopromide 300; Bayer Yakuhin, Ltd.).

MRI protocol. MRI was obtained using one of five 1.5-T or 3-T scanners: A Philips Achieva (Philips Healthcare), or a MAGNETOM Aera, MAGNETOM Prisma, MAGNETOM Skyra or MAGNETOM Verio (Siemens Healthineers), with a head coil or head-and-neck coil. Table I summarizes the MRI sequence parameters used. T1-weighted imaging (T1WI; using a spin-echo sequence) and short tau inversion recovery (STIR; turbo spin-echo sequence) images were acquired in both axial and coronal planes. The three-dimensional fast imaging sequence used for DCE-MRI featured the following parameters: Repetition time, 3.98-7.48 msec; echo time, 1.56-3.28 msec; and flip angle, 12°. Two consecutive scans were acquired as a prescan prior to contrast administration to check that the target lesion was within the imaging field, and to evaluate whether the images were affected by metal artifacts; the acquisition time for this prescan was 30 sec. Prior to the second scan of the first dynamic series, 0.1 ml/kg gadobutrol (Gadovist™; Bayer HealthCare Pharmaceuticals) was administered intravenously for 8 sec at a rate of approximately 2.0 ml/sec via automatic injection. The first image series, comprising 14 consecutive scans, was subsequently captured, with the acquisition time for each scan being 15 sec. Subsequently, a delay period of 180 sec without scanning was factored into the protocol, followed by two consecutive scans, each with an acquisition time of 15 sec. Another delay period of 180 sec was subsequently incorporated, followed by acquisition of the final two consecutive scans, again with an acquisition time of 15 sec each. The total scan time of this series was approximately 668 sec. CE T1-weighted images with fat saturation were acquired following DCE-MRI.

Evaluation of imaging features. Lesions were retrospectively evaluated on both CT and MRI scans by three oral and maxillofacial radiologists (with 5, 10 and 24 years of experience, respectively). The following features were evaluated for each lesion: The detectability of the lesion, the periphery of the lesion, the inner nature of the lesion, the density of the lesion on CT, the signal intensity of the lesion on MRI, the detectability of phleboliths, and shape of the lesion. Inter-observer differences were resolved by consensus. The detectability of lesions was classified as either positive or negative. The periphery of lesions was classified either as 'well-defined' or 'ill-defined'. The inner nature of the lesion was classified as 'homogeneous' or 'heterogeneous'. The density of the lesion on CT images was given one of the three following classifications: Hyperdense, isodense or hypodense. The signal intensity of the lesion on MRI was given one of the following four classifications, depending on the cerebral spinal fluid intensity: Markedly high, high, intermediate or low. The detectability of phleboliths was classified as either positive or negative. Finally, the shape of the lesion was classified into one of the following four categories: Mass, serpiginous vessel, dense capillaries, or a mixture of these categories (Fig. 1).

Table I. MRI parameters.

| | MRI sequence | | |
Imaging parameters	T1WI	STIR	CE-T1WI-FS
TR, msec	419-929	4,235-6,620	410-675
TE, msec	10-11	60-88	10-11
FOV, cm	18x18, 20x20, 22x22	18x18, 20x20, 22x22	18x18, 20x20, 22x22
Slice thickness, mm	2-5	2-5	2-5
Matrix size, pixels	384x348, 448x448, 512x512	320x320, 384x348, 448x448, 512x512	384x348, 448x448, 512x512

T1WI, T1-weighted imaging; STIR, short tau inversion recovery; CE-T1WI-FS, contrast-enhanced T1WI with fat saturation; TR, repetition time; TE, echo time; FOV, field of view.
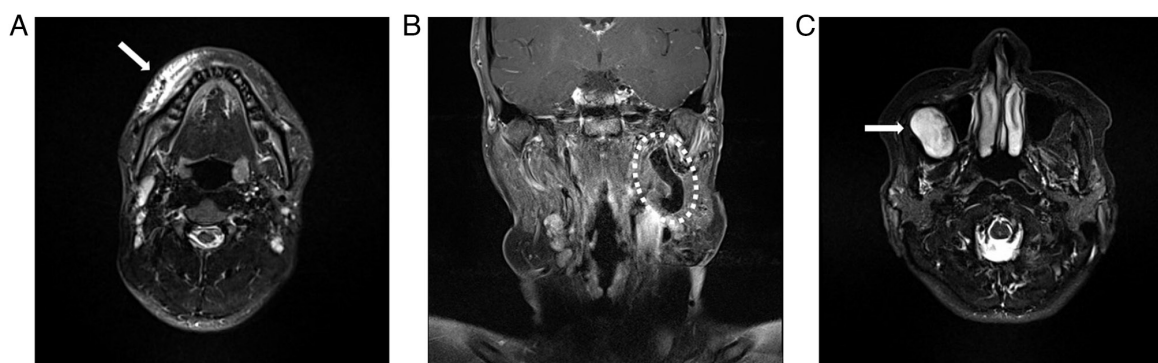

Figure 1. Shape categories of the vascular anomalies. (A) An axial STIR MR image, demonstrating markedly hyperintense dense small capillaries (white arrows) in the lower right buccal area. (B) A coronal T1-weighted MR image, demonstrating a hypointense serpiginous vessel (dashed circle) in the left maxillofacial area. (C) An axial STIR MR image, demonstrating a hyperintense mass (white arrows) in the right buccal area. MR, magnetic resonance; STIR, short tau inversion recovery.

Evaluation of DCE-MRI parameters. Lesions were further evaluated using DCE-MRI. For the 36 lesions with a suitable DCE-MRI acquisition, a region of interest (ROI) was manually drawn to include the greatest diameter of the lesion (Fig. 2A). The signal intensity of each lesion was subsequently calculated using a workstation (Synapse Vincent; Fujifilm Medical Co., Ltd.). The CI was subsequently calculated using the following formula:

$$CI = \frac{SI(post) - SI(pre)}{SI(pre)}$$

where SI(post) and SI(pre) represent the signal intensities within the ROI before and after the injection of contrast agent, respectively. The time course of the calculated CI was subsequently plotted, giving what termed the CI curve.

The following DCE-MRI parameters were derived from the CI curve: CI-max (i.e., the maximum level of contrast enhancement), T-max (i.e., the time taken to reach CI-max), CI-peak (i.e., the peak enhancement, which is equal to 0.9xCI-max), and T-peak (i.e., the time to reach the CI-peak). The T-peak parameter was calculated from the CI curve using the linear interpolation equation:

$$y = ya + \frac{(yb - ya)}{(xb - xa)} \times (x - xa)$$

where y is the known CI-peak, x is the unknown T-peak, (x, y) is the point to be obtained between point A and point B, point A=(xa, ya), and point B=(xb, yb); ya ≤ y ≤ yb.

The washout ratio at 300 sec (WR300), which is expressed as a percentage, was calculated using the following equation:

$$WR300 = \frac{CImax - CI300}{CI300} \times 100\%$$

where CI300 was also calculated using the CI obtained or linearly interpolated at 300 sec after T-max. We were not able to calculate the WR300 for those lesions in which the time course of their CI was <300 sec (this applied to seven of the lesions). Thus, we ultimately evaluated the CI curves of 29 lesions according to three parameters: CI-peak, T-peak and WR300 (Fig. 2B).

Diagnostic diagram construction. A diagnostic diagram was subsequently constructed, based on the imaging features of VAs and their CI curve patterns.

Results

Imaging features. The CT and MRI findings of the VAs are summarized in Table II. It was found that the lesions were most readily detectable on the STIR images, followed
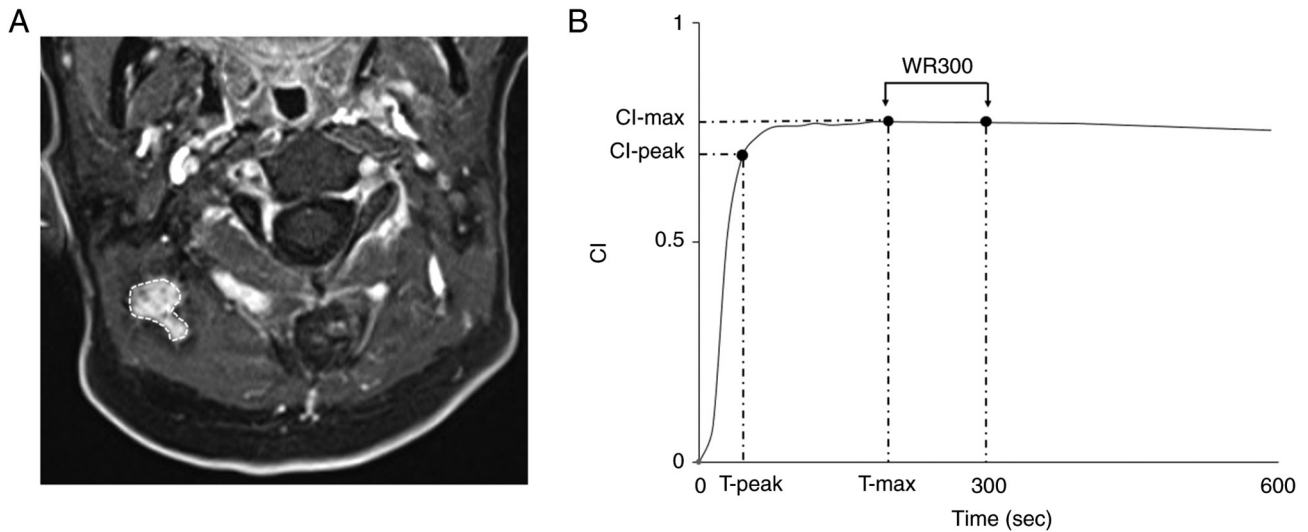
Figure 2. DCE-MRI image and typical CI curve of a vascular anomaly. (A) The region of interest (dashed line) drawn to include the region containing the greatest diameter of the lesion. (B) The CI curve of the lesion in Fig. 1A was constructed using DCE-MRI. CI, contrast index; DCE-MRI, dynamic contrast-enhanced magnetic resonance imaging.

by the CE-T1WI-FS, CE-CT, plain CT and T1WI images, respectively. Lesions tended to show ill-defined peripheries on T1WI images, whereas they tended to show well-defined peripheries on the STIR and CE-T1WI-FS images. In addition, lesions tended to show either well- or ill-defined borders on plain CT and CE-CT images. Moreover, lesions tended to show homogeneity on plain CT and T1WI images, whereas they tended to show heterogeneity on CE-CT, STIR and CE-T1WI-FS images. On plain CT, lesions tended to show isodensity, whereas on CE-CT, they tended to show hyperdensity. Furthermore, lesions tended to show intermediate signal intensity on T1WI, whereas they tended to show high signal intensity on STIR and CE-T1WI-FS images. Phleboliths were detected most readily on plain CT images, followed by CE-CT, CE-T1WI-FS, STIR and T1WI images, respectively. The majority of the lesions tended to show as a mass on both CT and MRI images, with one lesion showing as a serpiginous vessel, eight lesions showing as dense capillaries, and seven lesions showing as a mixed lesion of a mass and vessels.

CI curves. Fig. 3 shows our classifications of the CI curve patterns of 29 lesions. Twenty-three of the CI curves (79.3%), which showed early weak enhancement (CI-peak <2.0 and T-peak <200 sec) followed by a plateau phase, with this plateau being sustained for 400-600 sec, were classified as type A. Four of the CI curves (13.8%), which showed gradual weak enhancement (CI-peak <2.0 and T-peak >200 sec), were classified as type B. Only two lesions (6.9%) showed early strong enhancement (CI-peak >2.0 and T-peak <200 sec), and these were classified as type C; one of these showed strong washout (WR300 ≥30%), and was further subclassified as type CII. It should be noted that all of the lesions classified as types A, B or CI showed no, or minimal, washout (WR300 <30%).

Diagnostic diagram. The resulting imaging-based schematic diagram for diagnosing VAs is shown in Fig. 4. This diagram combines the imaging features and the CI curve patterns of oral and maxillofacial VAs.

Discussion

VAs can be found in any part of the head-and-neck region, and consequently, physicians often confuse these lesions with other types of lesion (19). The majority of physicians lack experience in diagnosing VAs (20), and therefore a successful diagnostic approach for VAs is essential to solve such challenges. The results obtained in the present study have indicated that VAs can be correctly diagnosed using a diagnostic diagram that combines imaging features of the lesion with a qualitative and quantitative analysis of their CI curves.

In general, CT images are excellent for detecting phleboliths within VAs (6). Kakimoto *et al* (6) found no significant differences between the techniques of CT and MRI in terms of the detection of VAs. However, it is not always easy to correctly differentiate between lesion tissue and surrounding tissues on CT scans (21). In addition, the role of CT is limited to bone assessment in the pediatric population due to the use of ionizing radiation (22). Therefore, as suggested by the findings of the present study, lesions are frequently underestimated on performing CT (23,24). By contrast, both the absence of ionizing radiation and the excellent soft-tissue contrast resolution afforded by MRI implies that this method may be the most valuable imaging modality for the diagnosis of VAs in many specialized healthcare units (2,24,25).

STIR images are a type of T2-weighted image with fat suppression, and are considered to be highly sensitive to fluid. Consequently, these sequences tend to be the most helpful in terms of lesion detection, as VAs contain high levels of fluid internally (26,27). Although fluids appear darker on T1WI images, the sequences generally have excellent spatial resolution, and are particularly useful for evaluating anatomical structures and tissue planes within VAs, as well as for characterizing the extent and anatomy of the VA if used prior to or after gadolinium administration (28). Therefore, the signal intensity of lesions in both T1WI and STIR images are considered to be essential for the detection of VAs.

Table II. Summary of the CT and MRI findings.

Imaging features	CT		MRI		
	CE (-)	CE (+)	T1WI	STIR	CE-T1WI-FS
Imaged lesions, n (%)	22 (100%)	15 (100%)	68 (100%)	87 (100%)	45 (100%)
Detectability, n (%)					
Positive	16 (72.7%)	12 (80%)	32 (47.1%)	87 (100%)	38 (84.4%)
Negative	6 (27.3%)	3 (20%)	36 (52.9%)	0 (0%)	7 (15.6%)
Periphery, n (%)					
Well-defined	8 (50%)	6 (50%)	12 (37.5%)	71 (81.6%)	23 (60.5%)
Ill-defined	8 (50%)	6 (50%)	20 (62.5%)	16 (18.4%)	15 (39.5%)
Inner nature, n (%)					
Homogeneous	9 (56.3%)	1 (8.3%)	29 (90.6%)	22 (25.3%)	4 (10.5%)
Heterogeneous	7 (43.8%)	11 (91.7%)	3 (9.4%)	65 (74.7%)	34 (89.5%)
Lesion density[a], n (%)					
Hyperdense	0 (0%)	10 (83.3%)	-	-	-
Isodense	15 (93.8%)	2 (16.7%)	-	-	-
Hypodense	1 (6.3%)	0 (0%)	-	-	-
Signal intensity[b], n (%)					
Markedly high	-	-	0 (0%)	26 (29.9%)	2 (5.3%)
High	-	-	1 (3.1%)	60 (69%)	31 (81.6%)
Intermediate	-	-	28 (87.5%)	0 (0%)	4 (10.5%)
Low	-	-	3 (9.4%)	1 (1.1%)	1 (2.6%)
Phleboliths, n (%)					
Positive	9 (56.3%)	5 (41.7%)	6 (18.8%)	17 (19.5%)	8 (21.1%)
Negative	7 (43.8%)	7 (58.3%)	26 (81.3%)	70 (80.5%)	30 (78.9%)
Lesion shape, n (%)					
Mass	15 (93.8%)	12 (100%)	29 (90.6%)	71 (81.6%)	33 (86.8%)
Serpiginous vessel	1 (6.3%)	0 (0%)	1 (3.1%)	1 (1.1%)	1 (2.6%)
Dense capillaries	0 (0%)	0 (0%)	1 (3.1%)	8 (9.2%)	1 (2.6%)
Mixed lesion	0 (0%)	0 (0%)	1 (3.1%)	7 (8%)	3 (7.9%)

T1WI, T1-weighted imaging; STIR, short tau inversion recovery; CE-T1WI-FS, contrast-enhanced T1WI with fat saturation; n, number of lesions. [a]Lesion density was evaluated on CT; [b]Signal intensity of lesions was evaluated on MRI.

Although the present study has provided novel insights into the association between CI curve parameters and VA diagnosis, a few other studies have already evaluated DCE-MRI findings in terms of diagnosing vascular lesions (19,25,29). Petea-Balea et al (19) determined that MRI with a DCE-MRI acquisition is the cornerstone imaging modality for the proper diagnosis of vascular lesions of the head-and-neck region. In addition, van Rijswijk et al (29) reported that DCE-MRI allows the diagnosis of venous malformations with high specificity. Moreover, Suenaga et al (30) suggested that dynamic curve patterns and the appearance of the tumor margin may help to differentiate among benign tumors, malignant tumors and inflammatory lesions.

In the protocol of DCE-MRI, the arrival of the contrast agent and the enhancement patterns of lesions depend on numerous factors, including vascularity, capillary permeability and the volume of the extravascular intercellular space. The analysis of contrast curves is able to provide a pertinent understanding of a lesion's composition, cellularity and vascular density. The analysis of CI curves can be performed according to the shape and morphology of the curve in a process known as qualitative analysis. Alternatively, it can be performed according to particular parameters derived from CI curves, such as CI-max, T-max, CI-peak, T-peak and washout rates (see above for a description of these parameters); this analysis is known as semi-quantitative analysis. The semi-quantitative analysis of CI curves, which we performed in the present study, is more robust than qualitative analysis, and also has the advantage of being independent of the injection protocol (31).

In the present study, the CI curve patterns of the VAs were classified according to three parameters: CI-peak, T-peak and WR300. Yabuuchi et al (32) reported that dynamic curve patterns classified according to the T-peak and the washout rate had high sensitivity and specificity in terms of differentiating benign tumors from malignant tumors. In the present study, the majority of the CI curves of the VAs exhibited an

Type A
CI-peak <2.0, T-peak <200 sec, WR300 <30%
n=23

Type B
CI-peak <2.0, T-peak >200 sec, WR300 <30%
n=4

Type CI
CI-peak >2.0, T-peak <200 sec, WR300 <30%
n=1

Type CII
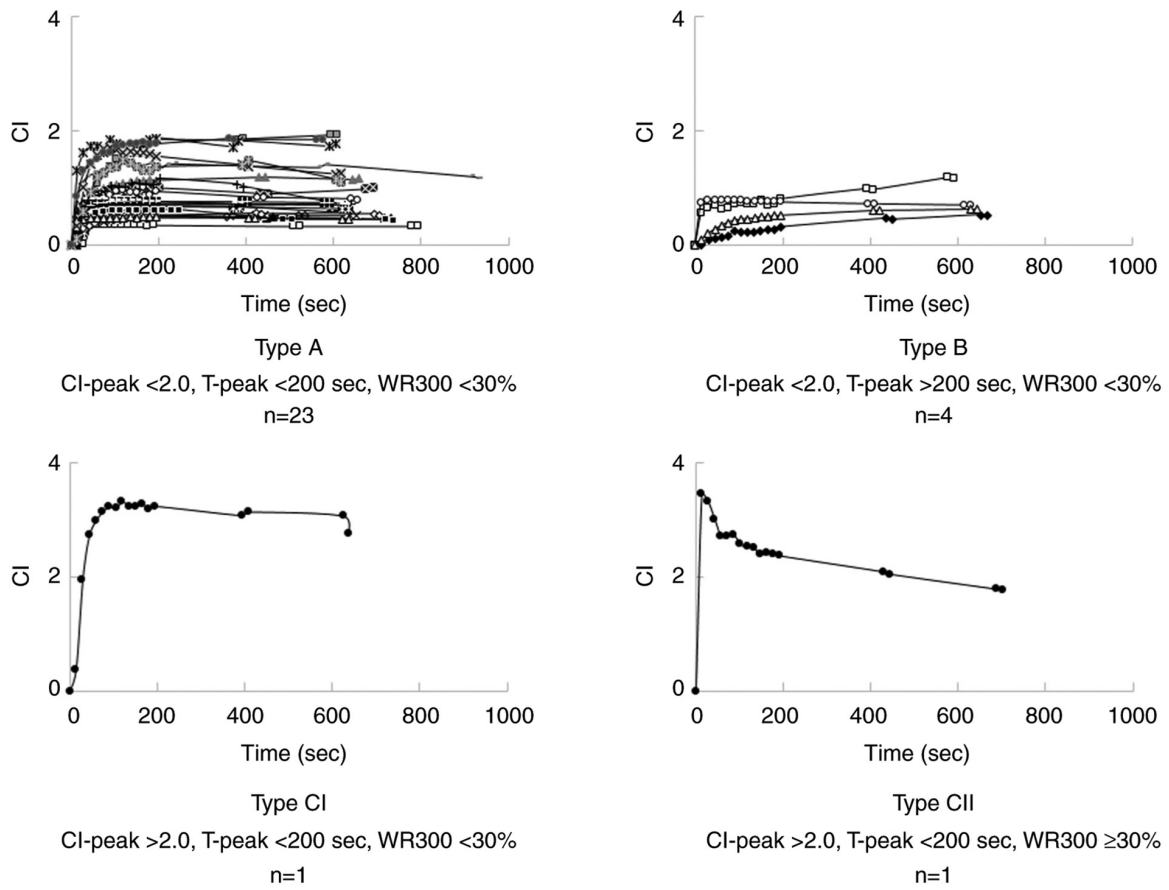CI-peak >2.0, T-peak <200 sec, WR300 ≥30%
n=1

Figure 3. Classification of the CI curve patterns. The CI curves were classified into four patterns (types A, B, CI and CII) on the basis of three parameters (CI-peak, T-peak, and WR300). Type A: Early weak enhancement; type B: Gradual weak enhancement; type CI: Early strong enhancement; type CII: Early strong enhancement with washout. CI, contrast index.
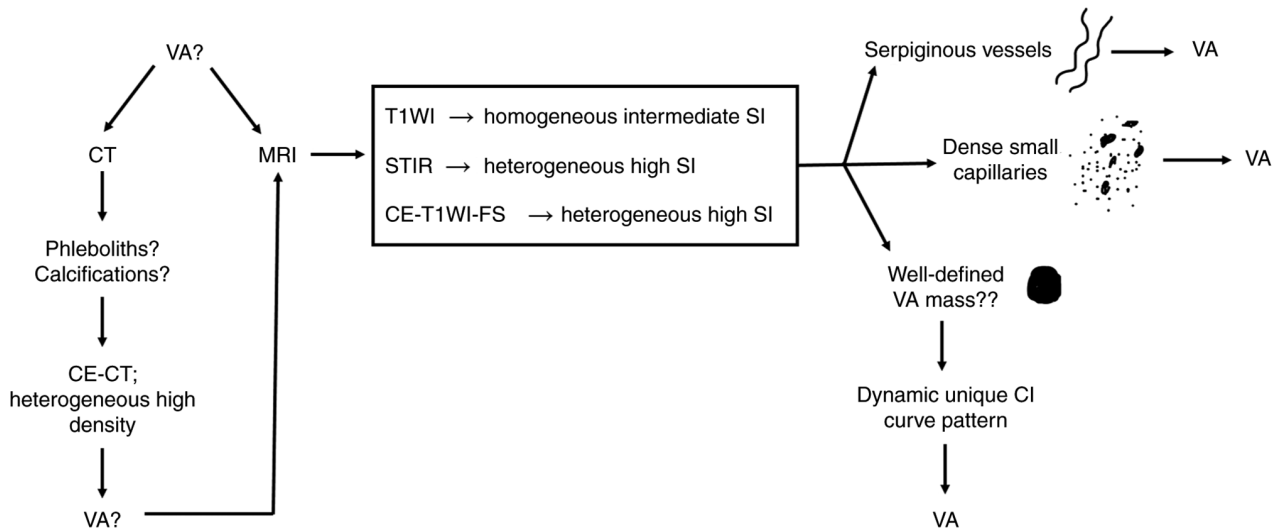

Figure 4. Imaging-based diagnostic diagram for VAs. VA, vascular anomaly; CE-CT, contrast-enhanced computed tomography; CE-T1WI-FS, contrast-enhanced T1-weighted imaging with fat saturation; SI, signal intensity; CI, contrast index; MRI, magnetic resonance imaging; STIR, short tau inversion recovery.

early peak of enhancement before 200 sec (T-peak <200 sec), with this enhancement peak being weak (CI-peak <2.0), after which the contrast intensity remained constant for a period of 400-600 sec, in what is known as the 'plateau phase'. Varidha *et al* (33) reported that a CI curve of rapid early enhancement followed by a plateau has limited specificity in terms of benign vascular lesion characterization. They also suggested early enhancement is a result of high micro-vascularization and tissue perfusion, whereas a plateau phase results from the accumulation of contrast in the neovasculature
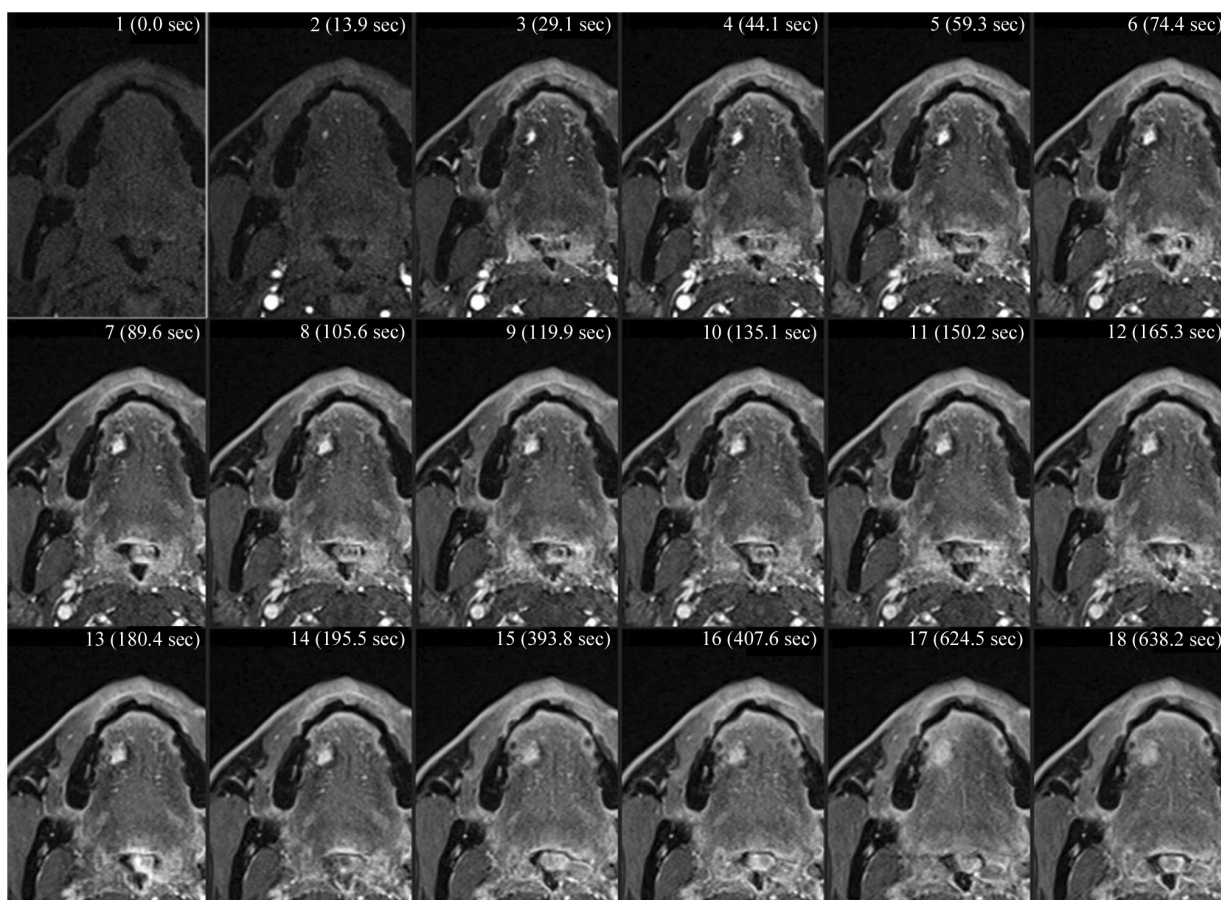
Figure 5. Central enhancement pattern of a vascular anomaly. DCE-MRI images of a vascular anomaly of the right tongue demonstrate gradual enhancement of contrast agent on the central portion of the lesion. DCE-MRI, dynamic contrast-enhanced magnetic resonance imaging.
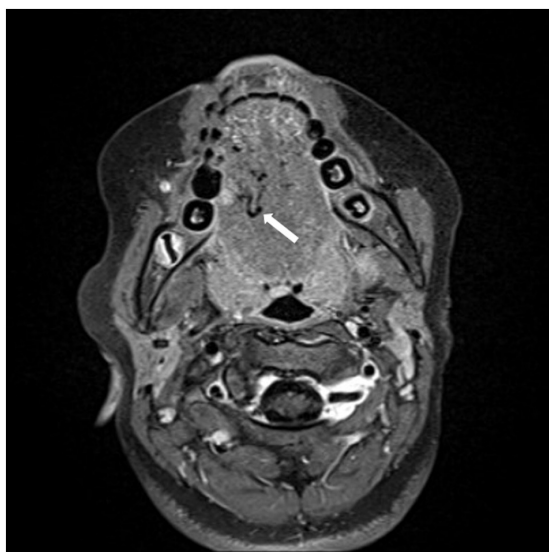

Figure 6. Incidental finding of a large-diameter vessel in a type CII vascular anomaly. The axial contrast-enhanced T1-weighted image with fat saturation is shown, demonstrating a large-diameter vessel (white arrow) in the right tongue.

and its surrounding interstitium due to a change in endothelial permeability. As a consequence, malignant tumors can also demonstrate early rapid enhancement followed by a plateau (34). However, previous studies that evaluated the CI curves of malignant tumors such as squamous cell carcinoma and Warthin tumors revealed that the contrast peak of the majority of malignant lesions is usually >2.0, which is much higher than the CI-peak of VAs (14,18).

Pleomorphic adenomas tend to share the same MRI features as VAs, presenting as a well-defined mass with the same inner nature and signal intensity as VAs on both T1WI and CE-T1WI-FS images (12). However, Hisatomi *et al* (12) reported that the CI curves of pleomorphic adenomas increased gradually to 600 sec, or increased gradually and reached a plateau that was sustained for 600 sec. In the present study, the CI curves of type B VAs showed a gradual increase up to 600 sec, although the CI-peaks of the type B lesions were <2.0, whereas the CI-peaks of the majority of pleomorphic adenomas are >2.0. Therefore, CI curves are able to distinguish VAs from pleomorphic adenomas.

Low-grade malignant salivary gland tumors tend to show similar MRI features to those of VAs, making them difficult to differentiate from each other (34). Moreover, the CI curves of malignant salivary gland tumors have similar patterns to those of type CI lesions, showing early strong enhancement (CI-peak >2) followed by a sustained plateau, with a WR300 value that is <30% (34). However, the CI curves of malignant salivary gland tumors usually show WR300 values of 10-30%, whereas the type CI lesions typically display a WR300 value <10% (34). Despite this difference, the WR300 parameter

alone is unreliable in terms of distinguishing this lesion from malignant salivary gland tumors, since the differences between the washout ratios are very subtle. However, in DCE-MRI, the enhancement pattern of the contrast agent exerts a key role in differentiating VAs from other types of malignancies. Malignant lesions tend to show peripheral contrast enhancement in DCE-MRI due to the presence of highly permeable microvessels that surround them (35,36), whereas VAs tend to show contrast enhancement from the center where the main vessels are located. Fig. 5 shows a typical contrast pattern of a VA in DCE-MRI.

We classified another lesion as type CII, which exhibited early strong enhancement followed by strong washout. This lesion was a mixed lesion with a large-diameter serpiginous vessel that had a high-dynamic-range blood flow rate, which indicated that the contrast agent flowed rapidly within the vessel, and as a result, the contrast washout rate of this lesion was strong (WR300 ≥30) (Fig. 6).

It should be noted that there were a number of limitations associated with this study. First, the use of multiple MRI and CT scanners for image acquisition could have been a limitation. Secondly, since the ROI placement was manually performed on the DCE images, this step in the protocol was susceptible to subjectivity in the choice of the images and selection of the appropriate ROI for each lesion. Thirdly, although the images of 87 VAs were utilized in the present study, having a larger dataset would have offered further insights.

In conclusion, the present study has demonstrated that VAs can be diagnosed using a diagnostic diagram based on their imaging features on performing CT, MRI, and DCE-MRI. The use of our diagram might enable the correct diagnoses of VAs to be made. The CI parameters derived from DCE-MRI contributed strongly to the differential diagnosis of VAs. Both the T-peak and WR300 values, and the morphology of the CI curve might be important in terms of differentiating VAs from pleomorphic adenomas. In addition, the CI-peak might be useful for distinguishing VAs from other types of malignant tumor, whereas WR300 alone is unreliable for differentiating VAs from malignant salivary gland tumors. In spite of this, it is possible to conclude that the enhancement pattern of the contrast agent on DCE-MRI might be the most reliable feature for differentiating VAs from other types of malignancies.

Acknowledgements

Funding

Availability of data and materials

The datasets used and/or analyzed during the current study are available from the corresponding author on reasonable request.

Authors' contributions

WEA, MamF, MH, MarF, YY and JIA conceived the ideas for the present study. WEA, MamF, MH, SO and JIA designed the study. MamF and MarF collected the patients' data for this study. WEA, MamF and TK confirm the authenticity of all the raw data. WEA, MamF, MH, LM, YT, TK and SO verified and performed the analytical methods. WEA, MamF and YT wrote the initial draft of the manuscript. JIA, MH, SO, LM, TK and YY edited the manuscript. All authors have read and approved the final manuscript.

Ethics approval and consent to participate

The study protocol was approved by the institutional review board of Okayama University Graduate School of Medicine, Dentistry and Pharmaceutical Sciences, Okayama University Hospital, Ethics Committee (approval no. 2209-024). The use of anonymized clinical data was explained in a document posted on the Okayama University Hospital website (https://www.okayama-u.ac.jp/user/orad/patients.html) to ensure that patients could choose to decline participation by the opt-out method. Informed consent for participation was obtained from every patient.

Patient consent for publication

Not applicable.

Competing interest

The authors declare that they have no competing interests.

References

1. Lee JW and Chung HY: Vascular anomalies of the head and neck: Current overview. Arch Craniofac Surg 19: 243-247, 2018.
2. Brahmbhatt AN, Skalski KA and Bhatt AA: Vascular lesions of the head and neck: An update on classification and imaging review. Insights Imaging 11: 19, 2020.
3. Samadi K and Salazar GM: Role of imaging in the diagnosis of vascular malformations. Cardiovasc Diagn Ther 9 (Suppl 1): S143-S151, 2019.
4. Legiehn GM and Heran MK: Classification, diagnosis, and interventional radiologic management of vascular malformations. Orthop Clin North Am 37: 435-474, vii-viii, 2006.
5. Kollipara R, Odhav A, Rentas KE, Rivard DC, Lowe LH and Dinneen L: Vascular anomalies in pediatric patients: Updated classification, imaging, and therapy. Radiol Clin North Am 51: 659-672, 2013.
6. Kakimoto N, Tanimoto K, Nishiyama H, Murakami S, Furukawa S and Kreiborg S: CT and MR imaging features of oral and maxillofacial hemangioma and vascular malformation. Eur J Radiol 55: 108-112, 2005.
7. Itoh K, Nishimura K, Togashi K, Fujisawa I, Nakano Y, Itoh H and Torizuka K: MR imaging of cavernous hemangioma of the face and neck. J Comput Assist Tomogr 10: 831-835, 1986.
8. Gelbert F, Riche MC, Reizine D, Guichard JP, Assouline E, Hodes JE and Merland JJ: MR imaging of head and neck vascular malformations. J Magn Reson Imaging 1: 579-584, 1991.
9. Sasaki Y, Sakamoto J, Otonari-Yamamoto M, Nishikawa K and Sano T: Potential of fluid-attenuated inversion recovery MRI as an alternative to contrast-enhanced MRI for oral and maxillofacial vascular malformations: Experimental and clinical studies. Oral Surg Oral Med Oral Pathol Oral Radiol 116: 503-510, 2013.
10. Zheng JW, Zhou Q, Yang XJ, Wang YA, Fan XD, Zhou GY, Zhang ZY and Suen JY: Treatment guideline for hemangiomas and vascular malformations of the head and neck. Head Neck 32: 1088-1098, 2010.
11. Nosher JL, Murillo PG, Liszewski M, Gendel V and Gribbin CE: Vascular anomalies: A pictorial review of nomenclature, diagnosis and treatment. World J Radiol 6: 677-692, 2014.

12. Hisatomi M, Asaumi J, Yanagi Y, Konouchi H, Matsuzaki H, Honda Y and Kishi K: Assessment of pleomorphic adenomas using MRI and dynamic contrast enhanced MRI. Oral Oncol 39: 574-579, 2003.
13. Matsuzaki H, Yanagi Y, Hara M, Katase N, Asaumi J, Hisatomi M, Unetsubo T, Konouchi H, Takenobu T and Nagatsuka H: Minor salivary gland tumors in the oral cavity: Diagnostic value of dynamic contrast-enhanced MRI. Eur J Radiol 81: 2684-2691, 2012.
14. Hisatomi M, Asaumi J, Konouchi H, Yanagi Y, Matsuzaki H and Kishi K: Assessment of dynamic MRI of Warthin's tumors arising as multiple lesions in the parotid glands. Oral Oncol 38: 369-372, 2002.
15. Asaumi J, Matsuzaki H, Hisatomi M, Konouchi H, Shigehara H and Kishi K: Application of dynamic MRI to differentiating odonto-genic myxomas from ameloblastomas. Eur J Radiol 43: 37-41, 2002.
16. Asaumi J, Yanagi Y, Konouchi H, Hisatomi M, Matsuzaki H and Kishi K: Application of dynamic contrast-enhanced MRI to differentiate malignant lymphoma from squamous cell carci-noma in the head and neck. Oral Oncol 40: 579-584, 2004.
17. Asaumi J, Yanagi Y, Konouchi H, Hisatomi M, Matsuzaki H, Shigehara H and Kishi K: Assessment of MRI and dynamic contrast-enhanced MRI in the differential diagnosis of adenoma-toid odontogenic tumor. Eur J Radiol 51: 252-256, 2004.
18. Tekiki N, Fujita M, Okui T, Kawai H, Oo MW, Kawazu T, Hisatomi M, Okada S, Takeshita Y, Barham M, et al: Dynamic contrast-enhanced MRI as a predictor of programmed death ligand-1 expression in patients with oral squamous cell carci-noma. Oncol Lett 22: 778, 2021.
19. Petea-Balea R, Lenghel M, Rotar H, Dinu C, Bran S, Onisor F, Roman R, Senila S, Csutak C and Ciurea A: Role of dynamic contrast enhanced magnetic resonance imaging in the diagnosis and management of vascular lesions of the head and neck. Bosn J Basic Med Sci 22: 156-163, 2022.
20. Ricci KW: Advances in the medical management of vascular anomalies. Semin Intervent Radiol 34: 239-249, 2017.
21. Wilmanska D, Antosik-Biernacka A, Przewratil P, Szubert W, Stefanczyk L and Majos A: The role of MRI in diagnostic algorithm of cervicofacial vascular anomalies in children. Pol J Radiol 78: 7-14, 2013.
22. McCafferty IJ and Jones RG: Imaging and management of vascular malformations. Clin Radiol 66: 1208-1218, 2011.
23. Jarrett DY, Ali M and Chaudry G: Imaging of vascular anoma-lies. Dermatol Clin 31: 251-266, 2013.
24. Bertino F, Trofimova AV, Gilyard SN and Hawkins CM: Vascular anomalies of the head and neck: Diagnosis and treatment. Pediatr Radiol 51: 1162-1184, 2021.
25. Lidsky ME, Spritzer CE and Shortell CK: The role of dynamic contrast-enhanced magnetic resonance imaging in the diagnosis and management of patients with vascular malformations. J Vasc Surg 56: 757-64.e1, 2012.
26. Nguyen TA, Krakowski AC, Naheedy JH, Kruk PG and Friedlander SF: Imaging pediatric vascular lesions. J Clin Aesthet Dermatol 8: 27-41, 2015.
27. Flors L, Leiva-Salinas C, Maged IM, Norton PT, Matsumoto AH, Angle JF, Bonatti MH, Park AW, Ahmad EA, Bozlar U, et al: MR imaging of soft-tissue vascular malformations: Diagnosis, clas-sification, and therapy follow-up. Radiographics 31: 1321-1340, discussion 1340-1341, 2011.
28. Legiehn GM and Heran MK: Venous malformations: Classification, development, diagnosis, and interventional radio-logic management. Radiol Clin North Am 46: 545-597, vi, 2008.
29. Van Rijswijk CS, van der Linden E, van der Woude HJ, van Baalen JM and Bloem JL: Value of dynamic contrast-enhanced MR imaging in diagnosing and classifying peripheral vascular malformations. AJR Am J Roentgenol 178: 1181-1187, 2002.
30. Suenaga S, Indo H and Noikura T: Diagnostic value of dynamic magnetic resonance imaging for salivary gland diseases: A preliminary study. Dentomaxillofac Radiol 30: 314-318, 2001.
31. Gordon Y, Partovi S, Müller-Eschner M, Amarteifio E, Bäuerle T, Weber MA, Kauczor HU and Rengier F: Dynamic contrast-enhanced magnetic resonance imaging: Fundamentals and application to the evaluation of the peripheral perfusion. Cardiovasc Diagn Ther 4: 147-164, 2014.
32. Yabuuchi H, Fukuya T, Tajima T, Hachitanda Y, Tomita K and Koga M: Salivary gland tumors: Diagnostic value of gado-linium-enhanced dynamic MR imaging with histopathologic correlation. Radiology 226: 345-354, 2003.
33. Varidha V, Rahardjo P and Setiawati R: The role of dynamic contrast enhancement MR imaging as a modality to differentiate between benign and malignant bone lesion. Int J Res Publ 57: 27-35, 2020.
34. Hisatomi M, Asaumi J, Yanagi Y, Unetsubo T, Maki Y, Murakami J, Matsuzaki H, Honda Y and Konouchi H: Diagnostic value of dynamic contrast-enhanced MRI in the salivary gland tumors. Oral Oncol 43: 940-947, 2007.
35. Ariyoshi Y and Shimahara M: Relationships between dynamic contrast-enhanced MRI findings and pattern of invasion for tongue carcinoma. Oncol Rep 15: 1339-1343, 2006.
36. Yıldırım A, Doğan S, Okur A, İmamoğlu H, Karabıyık Ö and Öztürk M: The role of dynamic contrast enhanced magnetic resonance imaging in differentiation of soft tissue masses. Eur J Gen Med 13: 37-44, 2016.